

## EXAMINING THE PRE-LANDFALL ENVIRONMENT OF MESOVORTICES WITHIN A HURRICANE BONNIE (1998) OUTER RAINBAND

[Scott M. Spratt](#)<sup>1</sup>, Frank D. Marks<sup>2</sup>, Peter P. Dodge<sup>2</sup>, and David W. Sharp<sup>1</sup>

<sup>1</sup>NOAA/National Weather Service Forecast Office, Melbourne, FL

<sup>2</sup>NOAA/AOML Hurricane Research Division, Miami, FL

### 1. INTRODUCTION

Tropical Cyclone (TC) tornado environments have been studied for many decades through composite analyses of proximity soundings (e.g. Novlan and Gray 1974; McCaul 1986). More recently, airborne and ground-based Doppler radar investigations of TC rainband-embedded mesocyclones have advanced the understanding of tornadic cell lifecycles (Black and Marks 1991; Spratt et al. 1997). This paper will document the first known dropwindsonde deployments immediately adjacent to a family of TC outer rainband mesocyclones, and will examine the thermodynamic and wind profiles retrieved from the marine environment. A companion paper (Dodge et al. 2000) discusses dual-Doppler analyses of these mesovortices.

On 26 August 1998, TC Bonnie made landfall as a category two hurricane along the North Carolina coast. Prior to landfall, two National Oceanographic and Atmospheric Administration (NOAA) Hurricane Research Division (HRD) aircraft conducted surveillance missions offshore the Carolina coast. While performing these missions near altitudes of 3.5 and 2.1 km, both aircraft were required to deviate around intense cells within a dominant outer rainband, 165 to 195 km northeast of the TC center. On-board radars detected apparent mini-supercell signatures associated with several of the convective cells along the band. A series of NOAA Global Positioning System dropsondes (Hock and Franklin, 1999) were launched from each aircraft, one of which descended directly through the reflectivity core of an outer rainband cell. Another dropsonde fell through a rain-free region between cells, near the southeastern end of the rainband. Data retrieved from these soundings will be discussed below.

### 2. RAINBAND AND CELL CHARACTERISTICS

National Weather Service (NWS) Weather Surveillance Radar- Doppler (WSR-88D) imagery from Morehead City, NC (KMHX) revealed that many of the cells within the dominant band could be categorized at the lower bound of the TC outer rainband mesocyclone spectrum defined by Sharp et al. (1997).

The Bonnie cells typically possessed 50 dBZ cores which extended aloft to near 4.3 km and tops to near 8.5 km. The cells were generally 18-28 km in diameter, with echo tops displaced about 11km downwind. While the individual cells along the rainband (shear axis) were identifiable for well over 1 h, observed rotational couplets were much less persistent, lasting an average of only 15 min., and confined to approximately the depth of the 50 dBZ echo.

### 3. MINI-SUPERCCELL DROPSONDE ANALYSIS

At 1602 UTC, a dropsonde was released immediately adjacent to a mini-supercell. Analysis of KMHX WSR-88D data suggests the cell had just completed a cycle of rapid (storm-relative) rotational spin-up/relaxation. The cell first revealed cyclonic rotation at lower levels between 1539 and 1544 UTC, peaked at 1549 UTC (15 m/s rotational velocity, .024 /s shear), then began to weaken rapidly after 1554 UTC. The indicated rotation was very shallow (below 2 km), with strongest

rotation shown near 1.1km.

Comparing radar reflectivity products with the dropsonde path, it appears that the sonde advected into the supercell shortly after release, then emerged downwind (southeast) of the cell just prior to reaching the surface. An equivalent potential temperature (Theta-e) profile ([Fig. 1](#)) revealed a steep lapse rate during descent, decreasing from 359 K at the sea surface until reaching a minima of 345 K at 500 m, indicative of a layer of surface-based conditional instability. Also through this depth, the mixing ratio (q; not shown) remained constant, near 21 g/kg, signifying the "mixed layer" as defined by Powell (1989). These Theta-e and q profiles were compared with those from a subset of seven dropsondes launched outside the rainband between 1530 and 2208 UTC, but within 100 km of the mini-supercell sonde. Each profile displayed much weaker Theta-e lapse rates and shallower mixed layers, with most possessing surface based neutral buoyancy with elevated layers of conditional instability.

A Convective Available Potential Energy (CAPE) of 1201 J/kg was obtained by bogusing thermodynamic quantities above flight level from the 1800 UTC MHX sounding (which was approximately 40 km from the supercell and within the rainband) and lifting the surface parcel. This degree of buoyancy greatly exceeds the average TC-tornado CAPE determined by McCaul (1991), but is only slightly larger than the CAPE computed for MHX.

The wind direction was found to veer with height from 108 degrees at sea level to 140 degrees just above the mixed layer ([Fig. 2](#)). Little change in direction occurred from 700 to 1700 m, with additional modest veering farther aloft. Wind speed increased rapidly within the same layer of pronounced veering, from 23 m/s at the surface to a relative maxima at 750 m of 44 m/s (not shown). Using the radar determined supercell motion of 147 degrees at 31.5 m/s and dropsonde winds yields a Storm-Relative Helicity (SRH) of  $392 \text{ m}^2/\text{s}^2$  within the 0-2 km layer and  $510 \text{ m}^2/\text{s}^2$  within the 0-3 km layer. Likewise, this extreme helicity is well above the average for TC events, and can be indicative of strong to violent (non-tropical) tornadoes (Davies-Jones et al. 1990).

#### **4. RAINBAND DROPSONDE ANALYSIS**

The dropsonde into the non-precipitative portion of the rainband was launched at 1728 UTC. KMHX storm-relative velocity images depicted low level convergence associated with a cell located 17 km downwind through 1745 UTC, followed by a period of rapid mesocyclogenesis. Observed rotational velocity peaked near 19 m/s (at a height of 1.1 km) at 1754 UTC. Rapid weakening then commenced, just before the cell reached the mainland coast. Notably, a cell possessing similar characteristics, located within the rainband, 45 km downwind from the circulation described above, moved onshore as a waterspout and produced F1 tornado damage at 1725 UTC.

The Theta-e profile showed a pronounced decrease of nearly the same magnitude as the supercell profile, but occurring through a much deeper layer, and elevated from 500 to 1300 m. A shallow mixed layer of 200 m was evident, in addition to a high surface q of 25 g/kg (not shown). A CAPE, calculated from the composite method described in section 3, of 1967 J/kg greatly exceeded the already excessive buoyancy of the supercell environment.

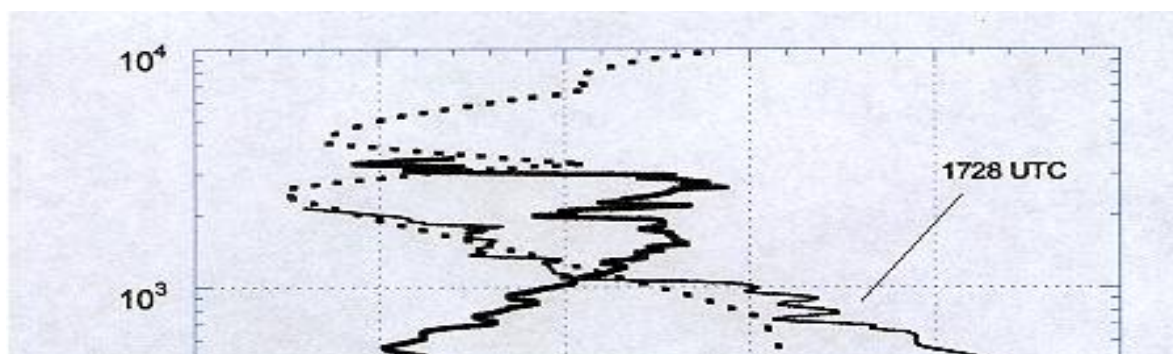
The wind direction varied slightly at lower levels, then veered from 132 degrees at the top of the mixed layer to 156 degrees at 950 m, with a slight backing evident between 500 and 600 m ([Fig. 2](#)). Farther aloft, the wind direction remained nearly constant. The degree of veering with height was quite similar to the supercell case, except winds were generally 20 degrees more easterly within the supercell profile. This difference accounted for a lower, although still impressive, 0-2 km SRH of  $177 \text{ m}^2/\text{s}^2$ .

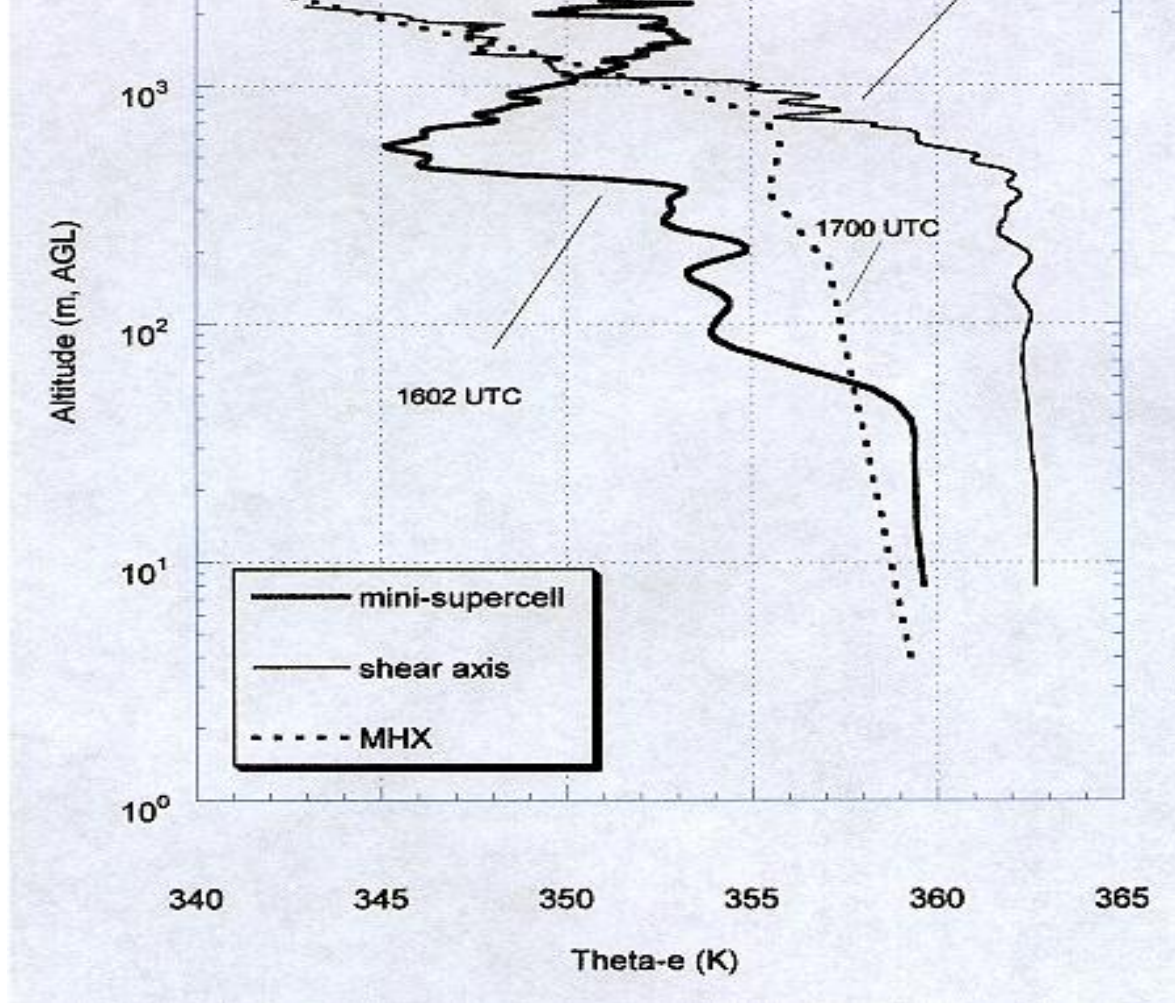
#### **5. CONCLUSIONS**

Thermodynamic quantities obtained from dropsondes within a TC Bonnie rainband revealed significant conditional instabilities and CAPE. Likewise, cell motions of nearly 80% of the mean 0-3 km wind yielded excessive SRH. Adjacent profiles outside the rainband displayed parameters less conducive to mesocyclone and tornado development. The large magnitude of local variability shown amongst the sondes emphasize the inability of the land-based radiosonde network to resolve the evolution of TC tornadic rainbands. To compensate, forecasters must closely monitor changes of cell structure within dominant rainbands via radar. Anticipating TC-supercell lifecycles may further heighten forecaster awareness and lengthen the lead-time for warnings.

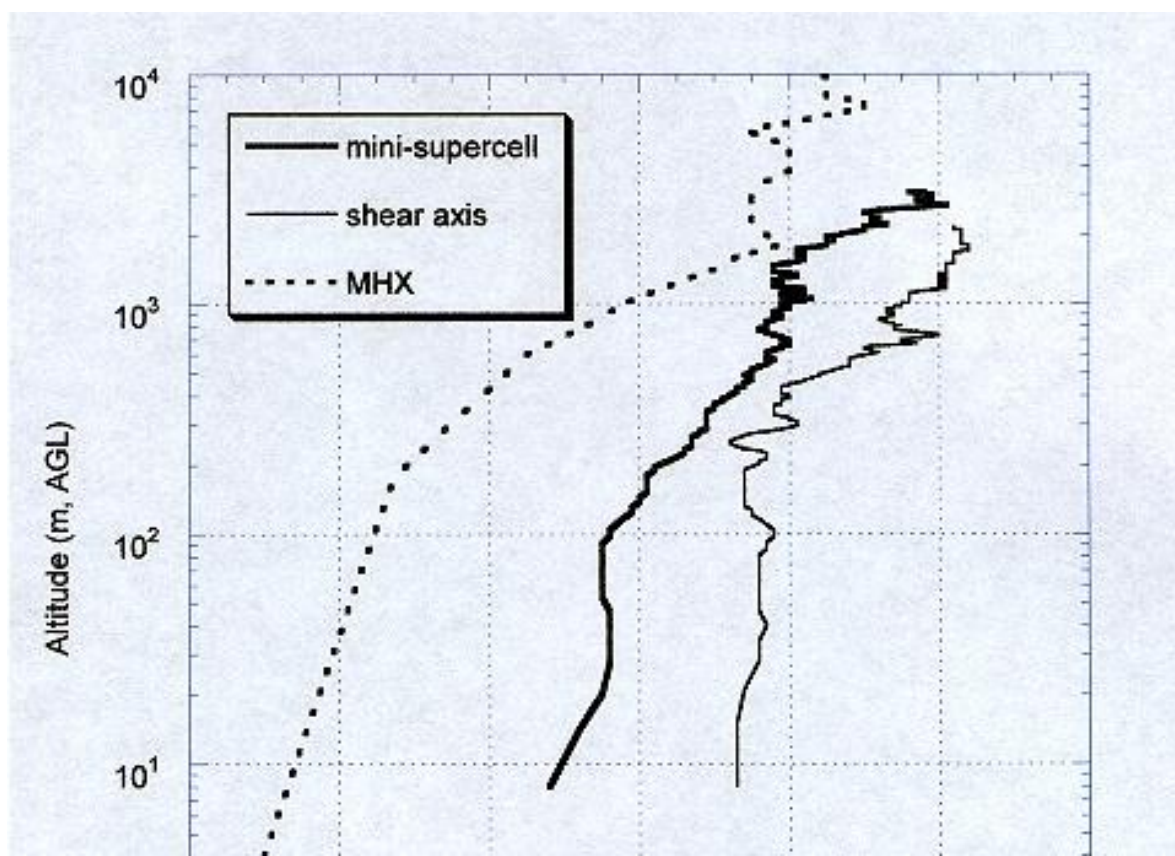
## 6. REFERENCES

- Black, P.G., and F.D. Marks, 1991: The structure of an eyewall meso-vortex in Hurricane Hugo (1989). Preprints, *15th Conf. on Hurricanes and Tropical Meteorology*, Miami, FL, Amer. Meteor. Soc., 579-582.
- Davies-Jones, R.P., D. Burgess, and M. Foster, 1990: Test of helicity as a tornado forecast parameter. Preprints, *16th Conf. on Severe Local Storms*, Kananaskis Park, AB, Canada, Amer. Meteor. Soc., 588-592.
- Dodge, P., S.M. Spratt, F.D. Marks, Jr., D.W. Sharp, and J. Gamache, 2000: [Dual-Doppler analyses of mesovortices in a hurricane rainband](#). Preprints, *24th Conf. on Hurricanes and Tropical Meteorology*, Ft. Lauderdale, FL, Amer. Meteor. Soc.
- Hock, T.F. and J.L. Franklin, 1999: The NCAR GPS Dropwindsonde. *Bull. Amer. Meteor. Soc.*, **80**, 407-420.
- Novlan, D.J. and W.M. Gray, 1974: Hurricane spawned tornadoes. *Mon. Wea. Rev.*, **102**, 476-488.
- McCaul, E.W., Jr. 1986: Observations of the Hurricane "Danny" tornado outbreak of 16 August 1985. *Mon. Wea. Rev.*, **115**, 1206-1223.
- McCaul, E.W., Jr., 1991: Buoyancy and shear characteristics of hurricane-tornado environments. *Mon. Wea. Rev.*, **119**, 1954-1978.
- Powell M.D., 1989: Boundary Layer Structure and Dynamics in Outer Hurricane Rainbands. Part II: Downdraft Modification and Mixed Layer Recovery. *Mon. Wea. Rev.*, **118**, 918-938.
- Sharp, D.W., J. Medlin, S.M. Spratt, and S.J. Hodanish, 1997: [A spectrum of outer spiral rainband mesocyclones associated with tropical cyclones](#). Preprints, *22nd Conference on Hurricanes and Tropical Meteorology*, Amer. Meteor. Soc., Ft. Collins, CO, pp 117-118.
- Spratt, S.M., D.W. Sharp, P. Welsh, A. Sandrik, F. Alsheimer, and C. Paxton, 1997: [A WSR-88D assessment of tropical cyclone outer rainband tornadoes](#). *Wea. Forecasting*, **12**, 479-501.





**Fig. 1.** Theta-e vertical profile obtained from NOAA aircraft dropsondes deployed adjacent to a mini-supercell and within rain-free region of the rainband. A special rawinsonde release from NWS MHX is shown for comparison. Sonde release times are shown.



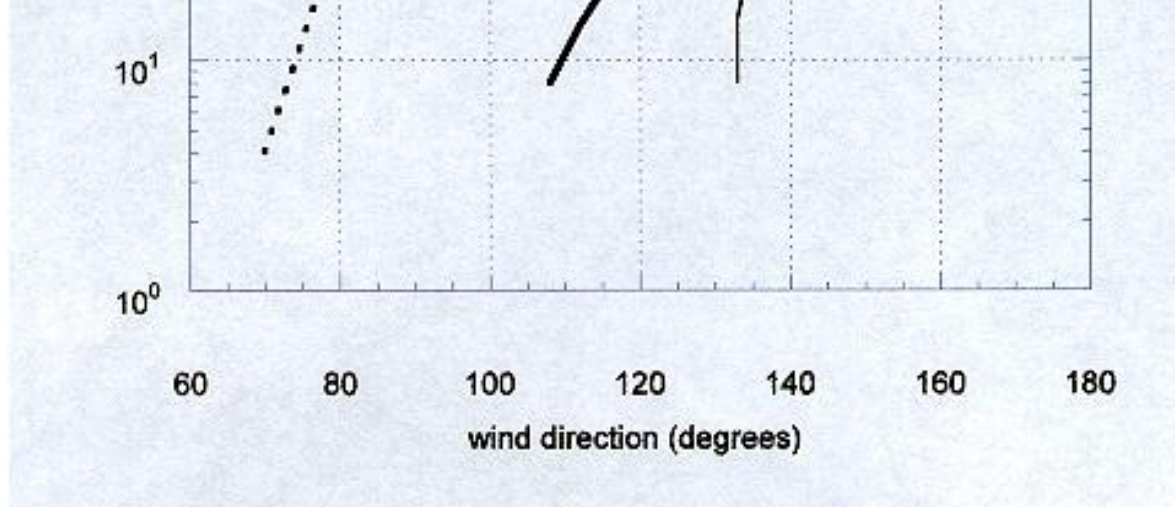


**Fig. 2.** Vertical profile of wind direction from same locations as Fig. 1